



universität
wien

MASTERARBEIT

Titel der Masterarbeit

”Numerical studies on coarse-grained quantum
measurements: Transition to classicality”

Autor

Matthias Kaiser B.Sc.

angestrebter akademischer Grad
Master of Science (M.Sc.)

Wien, 2012

Studienkennzahl lt. Studienblatt: A 066 876

Studienrichtung lt. Studienblatt: Physik

Betreuer: Ao. Univ.-Prof. Mag. Dr. Časlav Brukner

Danksagung

Als Erstes möchte ich meiner Familie danken, ohne deren Unterstützung diese Arbeit nicht möglich gewesen wäre. Weiter möchte ich Melanie Hudler danken, die mir beim Verfassen der Arbeit mit Rat und Tat beigestanden hat. Michael Epping danke ich für hilfreiche Diskussionen und Anregungen. Und zu guter Letzt natürlich Prof. Āaslav Brukner der mir die Möglichkeit gegeben hat diese Arbeit zu verwirklichen und mich nach Kräften unterstützt hat.

Contents

1	Introduction	1
2	Quantum physics and its mathematical foundation	2
2.1	Mathematical formalism	2
2.2	Postulates of quantum mechanics	4
2.3	Spin	8
2.4	Macroscopic spin systems	9
3	Crossing the borders of classical physics	11
3.1	EPR paradox	11
3.2	Bell inequality	12
3.3	CHSH inequality	12
3.4	Wigner inequality	15
3.5	Leggett-Garg inequality	16
3.6	Experimental violation of Bell type inequalities	17
4	Granularity	19
5	The Wigner-type Leggett-Garg inequality under coarse-grained measurements	20
5.1	Calculation of the Wigner expression K	21
5.2	Projective Slot Measurement (PSM)	22
5.3	Random Projection Measurement (RPM)	23
5.4	Numerical solution	24
5.5	Results	26
6	State disturbance due to coarse-grained measurements	30
6.1	Numerical solution	32
6.2	Results	32
7	Example for an implementation of coarse grained measurements in experiments	36
8	Conclusion	38
9	Outlook	39

1 Introduction

Since quantum mechanics was formulated in the beginning of the 20th century, many new effects were discovered and many new technologies invented. As well the philosophical and scientific world view as the technological progress were advanced by this new theory. Even though our modern world would be unthinkable without the techniques of quantum mechanics, many predictions and effects of quantum physics are still not well understood. In particular, the transition from quantum mechanics to classical physics and the measurement problem are still broadly discussed fields of scientific investigation.

In the present thesis, I will take a deeper look at how in special cases the transition between quantum mechanics and classicality is happening and at how coarse grained measurements can affect an initial state. In particular, I will investigate a smooth transition between fine-grained and very coarse-grained measurements.

First, I will give a brief introduction to the mathematical background and the fundamental postulates of quantum mechanics. Following this, we will see how classical physics and quantum mechanics can lead to incompatible predictions for measurement outcomes. Further, I will introduce the so called coarse grained measurements, which are measurements of finite precision. Subsequently, we will see to what extent coarse grained measurements can influence the state of a system and future evolutions. This will be based on the work of Johannes Kofler and Časlav Brukner [1], in which it was shown that one can observe genuine quantum-mechanical effects no matter how large the system is (i.e. how many particles it consist of). Furthermore, in their work it was shown that states that display quantum mechanical features under sharp measurements can appear classical when fuzzy measurements are made. Finally, I will show qualitatively the disturbance caused by projective measurements, by using the state disturbance measurement introduced by Asher Peres.

2 Quantum physics and its mathematical foundation

2.1 Mathematical formalism

Hilbert space

A Hilbert space \mathcal{H} is a complete, normed vector space (Banach space) with imaginary entries, where the inner product of two vectors ϕ and ψ is defined as $\langle \phi | \psi \rangle = \sum_{i=1}^n \phi_i^* \psi_i$, where star means the complex conjugated. The properties of the inner product are:

- $\langle \phi | \psi \rangle = \langle \psi | \phi \rangle^*$
- $\langle \phi | \lambda_1 \psi_1 + \lambda_2 \psi_2 \rangle = \lambda_1 \langle \phi | \psi_1 \rangle + \lambda_2 \langle \phi | \psi_2 \rangle$
- $\langle \lambda_1 \phi_1 + \lambda_2 \phi_2 | \psi \rangle = \lambda_1^* \langle \phi_1 | \psi \rangle + \lambda_2^* \langle \phi_2 | \psi \rangle$

with $\lambda_1, \lambda_2 \in \mathbb{C}$.

If the inner product of two vectors is zero we call these two vectors orthogonal to each other. A group of vectors that are in pairs orthogonal to each other is called an orthogonal system. A complete orthogonal system (no more vectors orthogonal to all the vectors in the orthogonal system can be found) is called an orthogonal base. If these vectors are normalized such that the inner product of any vector with itself is one, then we talk about an orthonormal base. Every Hilbert space has at least one orthonormal base and can be spanned by its orthonormal bases.

In section 2.2, I will explain how quantum mechanics and the mathematical structure of the Hilbert spaces are related to each other.

Dirac notation

Due to the fact that every Banach space has a dual space, also the Hilbert space \mathcal{H} has a dual space \mathcal{H}^* . As commonly used, we will also use the Dirac notation. In Dirac notation, any state vector $\psi \in \mathcal{H}$ is written as $|\psi\rangle$. The corresponding dual vector $\psi^* \in \mathcal{H}^*$ is written as $\langle \psi |$. The relation between vectors $|\psi\rangle$ and $\langle \psi |$ is injective and defined over the inner product as described in 2.1. More specifically, we can say that with $|\lambda\psi\rangle = \lambda|\psi\rangle$ and $\langle \lambda\psi | = \lambda^* \langle \psi |$ where $\lambda \in \mathbb{C}$, the image between \mathcal{H} and \mathcal{H}^* is antilinear:

$$\lambda_1 |\psi_1\rangle + \lambda_2 |\psi_2\rangle \longrightarrow \lambda_1^* \langle \psi_1 | + \lambda_2^* \langle \psi_2 | \quad (2.1)$$

with

$$\lambda_1, \lambda_2 \in \mathbb{C}; |\psi_1\rangle, |\psi_2\rangle \in \mathcal{H}; \langle \psi_1 |, \langle \psi_2 | \in \mathcal{H}^* \quad (2.2)$$

Linear operators

A linear operator \hat{A} assigns to any state vector $|\psi\rangle \in \mathcal{H}$ another state vector $|\psi'\rangle \in \mathcal{H}$, so that the relation between them is linear:

$$|\psi'\rangle = \hat{A}|\psi\rangle \quad (2.3)$$

The adjoint linear operator \hat{A}^\dagger assigns to any dual vector $\langle\psi| \in \mathcal{H}^*$ another dual vector $\langle\psi'| \in \mathcal{H}^*$ in the way

$$\langle\psi'| = \langle\psi|\hat{A}^\dagger \quad (2.4)$$

where dagger means the complex conjugated and transposed operator.

Any linear operator has the following properties for all choices of ψ :

- \hat{A} is equal to \hat{B} only if $\hat{A}|\psi\rangle = \hat{B}|\psi\rangle$
- $(\hat{A} + \hat{B})|\psi\rangle = \hat{A}|\psi\rangle + \hat{B}|\psi\rangle$
- $(\hat{A} \cdot \hat{B})|\psi\rangle = \hat{A}(\hat{B}|\psi\rangle)$
- In general, $\hat{A} \cdot \hat{B} \neq \hat{B} \cdot \hat{A}$ and we call $[\hat{A}, \hat{B}] = \hat{A} \cdot \hat{B} - \hat{B} \cdot \hat{A}$ the commutator
- If $[\hat{A}, \hat{B}] = 0$ we say that the operators \hat{A} and \hat{B} commute
- $\langle\phi|\hat{A}^\dagger|\psi\rangle = \langle\psi|\hat{A}|\phi\rangle^*$
- $(\hat{A}^\dagger)^\dagger = \hat{A}$
- $(\lambda\hat{A})^\dagger = \lambda^*\hat{A}^\dagger$
- $(\hat{A} + \hat{B})^\dagger = \hat{A}^\dagger + \hat{B}^\dagger$
- $(\hat{A} \cdot \hat{B})^\dagger = \hat{B}^\dagger \cdot \hat{A}^\dagger$

Further, we say that $|\psi\rangle$ is the eigenvector of the linear operator \hat{A} , if it fulfills the eigenvalue equality $\hat{A}|\psi\rangle = \lambda|\psi\rangle$ with the eigenvalue $\lambda \in \mathbb{C}$. The whole set of solutions λ for \hat{A} is called the spectra of \hat{A} .

Projection operators

A special and for representation of quantum measurements very important type of linear operators are the projectors. All projectors \hat{P} can be written in the form $\hat{P} = |\psi\rangle\langle\psi|$. If we apply operator \hat{P} to another space state vector $|\chi\rangle$ we get

$$\hat{P}|\chi\rangle = |\psi\rangle\langle\psi|\phi\rangle = c \cdot |\psi\rangle \quad (2.5)$$

where $c = \langle\psi|\phi\rangle$. This gives us the projection of the vector $|\phi\rangle$ on the vector $|\psi\rangle$ (see scheme 2.1).

The projection operator has then the properties:

- $\hat{P}^2 = \hat{P}$
- $\hat{P}^\dagger = \hat{P}$

The projectors are Hermitian operators meaning that the eigenvalues of these operators are real and can be interpreted as observables of a physical system.

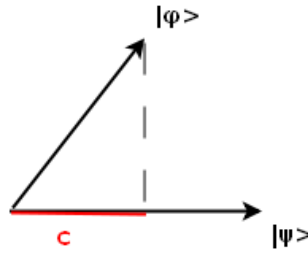


Figure 2.1: Scheme of the projection.

2.2 Postulates of quantum mechanics

We will now describe how the mathematical formalism of quantum mechanics is related to the observations of the physical world.

For further reading I recommend [2].

Postulate 1: State space

The first postulate defines the space of physical states in quantum mechanics.

Postulate 1: "Associated to any isolated physical system is a complex vector space with inner product (that is, a Hilbert space) known as the state space of the system. The system is completely described by its state vector, which is a unit vector in the system's state space." [2]

In general, every state vector $|\psi\rangle$ in a state space can be written as the sum (superposition) of the state space basis vectors $|\phi_i\rangle$ with the corresponding complex amplitudes α_i

$$|\psi\rangle = \sum_i \alpha_i |\phi_i\rangle, \quad (2.6)$$

With the condition that $|\psi\rangle$ is the unit vector, we get $\langle\psi|\psi\rangle = 1$ and therefore $\sum_i |\alpha_i|^2 = 1$. This is also called the normalization condition.

The simplest quantum mechanical system is the two level system, also called qubit. The complete basis for this state space can be written as $|0\rangle$ and $|1\rangle$. In this notation any arbitrary state vector can be represented by:

$$|\psi\rangle = \alpha|0\rangle + \beta|1\rangle, \quad (2.7)$$

where again $|\alpha|^2 + |\beta|^2 = 1$.

Every state of a two-level systems can be represented as a vector within or on a three-dimensional unit sphere, the so-called Bloch sphere, on which are all pure states for a closed system. Taking the following representation of a pure state:

$$|\psi\rangle = \cos\left(\frac{\theta}{2}\right)|0\rangle + e^{i\varphi} \sin\left(\frac{\theta}{2}\right)|1\rangle \quad (2.8)$$

One can identify every state with a point (θ, ϕ) on the sphere. Here, θ gives the rotation-angle in the x - z -plane and φ (which is the phase between the amplitudes of $|0\rangle$ and $|1\rangle$) is the rotation angle in the x - y -plane.

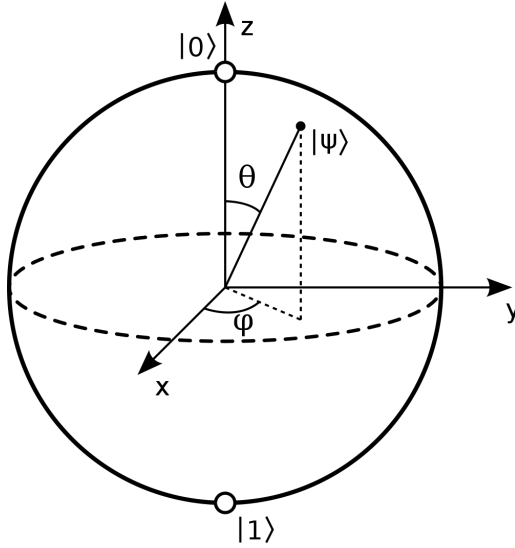


Figure 2.2: Illustration of the Bloch sphere.(Illustration taken from [3])

Postulate 2: Time evolution

Next we will describe how the dynamics of a quantum-mechanical state can be described, i.e. how a state vector evolves with time. The second postulate describes this time evolution.

Postulate 2: "The evolution of a closed quantum system is described by an unitary transformation. That is, the state $|\psi\rangle$ of the system at time t_1 is related to the state $|\psi'\rangle$ of the system at time t_2 by a unitary operator \hat{U} which depends only on the times t_1 and t_2 ,

$$|\psi'\rangle = \hat{U}|\psi\rangle." [2] \quad (2.9)$$

In terms of the Bloch sphere, it means that every possible unitary time evolution can be represented by rotations of the state vector around the axes of the Bloch sphere.

Postulate 2 defines how the state evolves after the application of a given unitary transformation. A continuous transformation of the system in time is governed by the Schrödinger equation as follows:

$$i\hbar \frac{\partial |\psi\rangle}{\partial t} = \hat{H}|\psi\rangle. \quad (2.10)$$

Here \hbar is the Planck constant, we choose the units such that $\hbar = 1$. \hat{H} is called the Hamiltonian. With the knowledge of \hat{H} , we can completely determine the evolution of the system $|\psi\rangle$.

The connection between the Hamiltonian and the unitary operator is given by:

$$U(t_1, t_2) = e^{-i\hat{H}(t_2-t_1)}, \quad (2.11)$$

where we consider a time-independent Hamiltonian.

Postulate 3: Quantum mechanical measurement

Until now we have discussed the set of states of a closed system and its temporal evolution. In classical physics, the complete information about the state and its evolution, would be enough to predict deterministically future measurement outcomes. In quantum mechanics this is not the case, and the prediction which measurement outcome will occur is fundamentally probabilistic. So unlike in classical physics, the measurement process is of great importance. Postulate 3 defines this process and its effect on the quantum state.

Postulate 3: "Quantum measurements are described by a collection $\{\hat{M}_m\}$ of measurement operators. These are operators acting on the state space of the system being measured. The index m refers to the measurement outcomes that may occur in the experiment. If the state of the system is $|\psi\rangle$ immediately before the measurement then the probability that result m occurs is given by

$$p_m = \langle \psi | \hat{M}_m^\dagger \hat{M}_m | \psi \rangle, \quad (2.12)$$

and the state of the system after the measurement is

$$|\psi_m\rangle = \frac{\hat{M}_m |\psi\rangle}{\sqrt{\langle \psi | \hat{M}_m^\dagger \hat{M}_m | \psi \rangle}}. \quad (2.13)$$

The measurement operators satisfy the completeness equation,

$$\sum_m \hat{M}_m^\dagger \hat{M}_m = \mathbb{1}." [2] \quad (2.14)$$

The completeness equation means that the sum over all possibilities add up to 1:

$$\sum_m p_m = \sum_m \langle \psi | \hat{M}_m^\dagger \hat{M}_m | \psi \rangle = 1. \quad (2.15)$$

Projective measurements

A very important kind of measurement for many applications is the projective measurement. For these measurements, the measurement operators \hat{M}_d are replaced by the projection operators \hat{P}_d as introduced in 2.1. The projector \hat{P}_d can be seen as a projection on any vector $|d\rangle$ and can be written as:

$$\hat{P}_d = |d\rangle\langle d| \quad (2.16)$$

This projectors correspond to the measurement outcome d . The projection operators \hat{P}_d build the spectral decomposition of an observable \hat{O} we want to measure:

$$\hat{O} = \sum_d d \cdot \hat{P}_d = \sum_d d \cdot |d\rangle\langle d|, \quad (2.17)$$

whereby \hat{P}_d is a projector on the eigenspace of \hat{O} and the d is the corresponding eigenvalue. The existence of this spectral decomposition means that $|d\rangle$ span an orthonormal basis, and thus that the projection operators \hat{P}_d are orthogonal. One therefore has

$$\hat{P}_d \hat{P}_{d'} = \delta_{dd'} \hat{P}_d. \quad (2.18)$$

If we choose the M_m in Postulate 3 to be orthogonal, we end up with projective measurements.

The probability for one specific outcome for a measurement on the state $|\psi\rangle$ is then given by:

$$p_d = \langle \psi | \hat{P}_d | \psi \rangle \quad (2.19)$$

And the state after the measurement is:

$$|\psi_d\rangle = \frac{\hat{P}_d |\psi\rangle}{\sqrt{p_d}} \quad (2.20)$$

The average value of the observables is

$$E(\hat{O}) = \sum_d d \cdot p_d \quad (2.21)$$

$$= \sum_d d \cdot \langle \psi | \hat{P}_d | \psi \rangle \quad (2.22)$$

$$= \langle \psi | \left(\sum_d d \cdot \hat{P}_d \right) | \psi \rangle \quad (2.23)$$

$$= \langle \psi | \hat{O} | \psi \rangle. \quad (2.24)$$

This easy way of calculating average values can be a very helpful tool.

Positive Operator Valued Measurements

Positive Operator Valued Measurements (POVM) are the most general formulation of measurements in quantum physics. POVM are self-adjoint operators and their values are non-negative.

If we define $E_m = M_m M_m^\dagger$, then the properties of Postulate 3 are

$$\sum_m E_m = \mathbb{1} \quad (2.25)$$

and

$$p_m = \langle \psi | E_m | \psi \rangle. \quad (2.26)$$

The operators E_m are called the POVM elements and the complete set $\{E_m\}$ is called a POVM. The E_m are positive and give the probability of the corresponding measurement outcome if applied to a state. As long as the POVM elements are positive and fulfill the completeness relation the POVM can be chosen freely.

POVM can be a very helpful tool for state discrimination, in which two or more states can be distinguished in a one-shot-experiment.

2.3 Spin

An important property of particles is the so called spin. The spin is analogue to the mechanical angular momentum except that it is not caused by the rotation of a mass but is an intrinsic quantum property. As Otto Stern and Walther Gerlach proved with their experiment performed in Frankfurt/Main in 1922, the spin is quantized. With the emergence of quantum mechanics it became very clear that the spin can be explained only in terms of quantum mechanics.

The spin plays a very important role in atomic physics. For example, the spin of the electron has a big influence on the formation of molecules and on the appearance of matter.

In general, two different families of particles can be distinguished, namely fermions with half-integer and bosons with integer spin. Due to spin conservation, restrictions for the decay of particles are emerging. These restrictions are very important in atomic and particle physics. For our further investigations, we will deal with fermions only. Furthermore, we will limit our calculations to fermions with spin $1/2$, which could be electrons, for example.

If the spin of such a particle should be measured, the procedure is to choose a probing axis and then measure the spin quantum-number m_s along this axis. This gives the "direction in which the rotation axis of the spin is pointing" and we call it "spin-up" and "spin-down". The values correspond to $m_s = \pm 1/2$, respectively. In Dirac notation, we can write $|\uparrow\rangle$ and $|\downarrow\rangle$ or $|1\rangle$ and $|0\rangle$. In vector notation, one has $\begin{pmatrix} 1 \\ 0 \end{pmatrix}$ and $\begin{pmatrix} 0 \\ 1 \end{pmatrix}$. In quantum computation this is also called a computational or binary basis.

Obviously the Hilbert-space of spin- $1/2$ particles is two dimensional. As we noticed in 2.2, all unitary transformations can be seen as rotations on the Bloch sphere. In the two dimensional case all these rotations can be implemented by using the Pauli-matrices, where the index tells us the axis around which the state vector is rotated. The Pauli-matrices are:

$$\sigma_x = \begin{pmatrix} 0 & 1 \\ 1 & 0 \end{pmatrix}; \sigma_y = \begin{pmatrix} 0 & -i \\ i & 0 \end{pmatrix}; \sigma_z = \begin{pmatrix} 1 & 0 \\ 0 & -1 \end{pmatrix} \quad (2.27)$$

with the property

$$\sigma_i \sigma_j = \delta_{ij} \cdot \mathbb{1} + i \sum_k \epsilon_{ijk} \sigma_k. \quad (2.28)$$

where δ_{ij} is the Kronecker-delta and ϵ_{ijk} is the Levi-Civita symbol.

These matrices are hermitian and unitary and together with the unit matrix they span the full vector space of all hermitian 2×2 matrices. This means that all hermitian operations on a two dimensional system can be decomposed into a combination of the Pauli matrices and the unit matrix. All unitary operators on a two-level system can be written in the following form:

$$U = e^{i\phi} e^{i\alpha\sigma_i} e^{i\beta\sigma_j} e^{i\gamma\sigma_k}, \quad (2.29)$$

where the i, j, k can be equal or different, the α, β, γ are the angles of rotation and ϕ gives an additional phase. Therefore, a rotation for the

angle α around the i -axis is

$$U_i(\omega) = e^{-i\alpha\sigma_i} = \mathbb{1} \cos \alpha - i\sigma_i \sin \alpha. \quad (2.30)$$

Proof:

$$e^{-i\alpha\sigma_i} = \sum_{n=0}^{\infty} \frac{i^n (-\alpha \cdot \sigma_i)^n}{n!} \quad (2.31)$$

$$= \sum_{n=0}^{\infty} \frac{(-1)^n (-\alpha \cdot \sigma_i)^{2n}}{(2n)!} - i \sum_{n=0}^{\infty} \frac{(-1)^n (\alpha \cdot \sigma_i)^{2n+1}}{(2n+1)!} \quad (2.32)$$

$$= \mathbb{1} \cos \alpha - i\sigma_i \sin \alpha \quad (2.33)$$

Where we used the Taylor series and the property 2.28 for the Pauli matrices.

As an example we give the rotation matrix around the y-axis:

$$U_y(\alpha) = \begin{pmatrix} \cos \alpha & -\sin \alpha \\ \sin \alpha & \cos \alpha \end{pmatrix} \quad (2.34)$$

This transformation applied on the basis set states gives:

$$U_y \cdot |\uparrow\rangle = \cos \alpha |\uparrow\rangle + \sin \alpha |\downarrow\rangle \quad (2.35)$$

$$U_y \cdot |\downarrow\rangle = -\sin \alpha |\uparrow\rangle + \cos \alpha |\downarrow\rangle \quad (2.36)$$

2.4 Macroscopic spin systems

We will now describe a "macroscopic spin system", a composite quantum system that consists of a large number N of single spins. Such a macroscopic spin system could be a particle cloud. If the individual spin states are pure and separable the Hilbert space of the composite system has the dimension $D = 2^N$ and the state of such a system is given by:

$$|\Psi\rangle = |\psi_1\rangle \otimes |\psi_2\rangle \otimes |\psi_3\rangle \otimes \dots \otimes |\psi_N\rangle. \quad (2.37)$$

One particular such macroscopic spin state could be:

$$|\Psi_S\rangle = |\uparrow, \downarrow, \uparrow, \uparrow, \downarrow, \dots\rangle \quad (2.38)$$

I will refer to states of such kind as states in spin basis.

If the spins are in an entangled state it is hard to analytically analyze such systems due to the large dimensionality of the Hilbert space.

If we are dealing with indistinguishable spin particles the information about "which particle is in which state" should not be accessible in the quantum state. In this case we can use the total spin projection along an axis, say z-axis, M as a representation for the state. Note that the states $|\uparrow, \downarrow, \uparrow\rangle$ and $|\uparrow, \uparrow, \downarrow\rangle$ for example would have the same projection of the total spin quantum-number $M = 1/2$. The state of the composite system can thus be written as the superposition of the corresponding states with the same spin quantum-number. In our example $|M = 1/2\rangle = \frac{1}{\sqrt{3}} \cdot (|\uparrow, \uparrow, \downarrow\rangle + |\uparrow, \downarrow, \uparrow\rangle)$

$\rangle + |\downarrow, \uparrow, \uparrow\rangle$). Likewise any other $|M\rangle$ can be constructed.

For our purposes we will use a slightly different notation. Due to the fact that the number of particles with spin-up and spin-down defines the value of M , we can write the state as $|(N-p)_{up}, p_{down}\rangle$, whereby N is the total number of particles and p is the number of particles with spin down. Our state can thus in general be written as

$$|(N-p)_{up}, p_{down}\rangle = \frac{1}{\sqrt{\binom{N}{p}}} \cdot \sum_{i=1}^{\binom{N}{p}} S_i[|\uparrow\rangle^{\otimes(N-p)} \otimes |\downarrow\rangle^{\otimes p}], \quad (2.39)$$

whereby $S_i[|\uparrow\rangle^{\otimes(N-p)} \otimes |\downarrow\rangle^{\otimes p}]$ gives the permutations for all possible spin configurations at a given N and p . The set of basis vectors of the composite system we will call the reduced basis. It can easily be checked that the resulting Hilbert space for the symmetric subspace spanned by states 2.39 is just $N+1$ dimensional, not 2^N as for distinguishable particles.

3 Crossing the borders of classical physics

3.1 EPR paradox

In the beginning of the 20th century the first hints towards quantum mechanics were discovered, like the quantization of light in Max Planck's radiation law or the quantization of the electron trajectory in the atomic model of Niels Bohr. Physicists were endeavored to integrate the new findings into the ruling realistic world view, according to which a result of a measurement is existing regardless of whether a measurement is performed or not. In the 1920th and 30th, Werner Heisenberg, Erwin Schrödinger, Max Born, Pascual Jordan, Wolfgang Pauli, Nils Bohr, Paul Dirac, John von Neumann, Friedrich Hund and others formulated the quantum theory. At this time many effects of quantum physics, like the tunnel effect or the quantization of light, were already discovered, but no underlying theory was formulated. With the matrix mechanics of Heisenberg and the wave mechanics of Schrödinger it was now possible to make precise predictions.

The theory gave only probabilities for the occurrence of outcomes when a system is measured. This was in direct contrast to the predominant world view and classical physics. On the basis of certain set of assumption in agreement with the classical world view Albert Einstein, Boris Podolsky and Nathan Rosen came to the result that quantum mechanics cannot be a complete theory.

In summary, the four main assumptions of Einstein, Podolsky and Rosen are [4]:

Perfect (anti-)correlation: "...by measuring either A or B we are in a position to predict with certainty, and without in any way disturbing the second system, either the value of the quantity P or the value of the quantity Q." (remark: A and B are properties of particle 1 and P and Q are properties of particle 2, whereby P and Q do not commute.)

Locality: "Since at the time of measurements the two systems no longer interact, no real change can take place in the second system in consequence of anything that may be done to the first system."

Reality: "If, without in any way disturbing a system, we can predict with certainty (i.e., with probability equal to unity) the value of a physical quantity, then there exists an element of physical reality corresponding to this physical quantity."

Completeness: "Every element of the physical reality must have

a counterpart in the [complete] physical theory.”

To find a complete theory, that would contain the predictions of quantum mechanics, the so-called hidden variable theories were suggested. These hidden variables should contain the information that is necessary to predict the outcomes of all possible measurement on a (multipartite) system.

3.2 Bell inequality

Ever since the birth of quantum theory the discussions whether or not quantum mechanical description is complete were based on philosophical arguments. Besides, most physicists concentrated more on the practical side of the new theory. This changed in 1966 when John Stuart Bell published a paper [5], in which he gave his analysis of the EPR discussion and presented an inequality which could experimentally distinguish between a local realistic (hidden variable) theory and the predictions of quantum mechanics. The philosophical question became finally verifiable in experiments.

Based on the assumptions of the EPR paper, Bell constructed an inequality satisfied by the correlations in any local realistic theory. If this bound is violated no local realistic theory can describe the correlations between the measured systems. We will discuss more in detail in 3.3 how this inequality is constructed.

3.3 CHSH inequality

On the basis of the Bell’s work, John F. Clauser, Michael A. Horne, Abner Shimony and Richard A. Holt (CHSH) formulated an inequality that is valid also in the case of not perfectly correlated systems [6]. To understand this inequality we will make a gedanken experiment.

Imagine a source that emits two particles. These particles are then sent, one to Alice and one to Bob where they are detected. The two observers are space-like separated. In front of each detector, there is a device with which one can choose which property of the particle will be measured, the so called setting. The detectors can record the binary outcomes ± 1 (see fig. 3.1). As an illustration of the measurement one could imagine a spin measurement. The setting gives the direction along which the spin is measured and the detector give us the information if the spin is up or down. Alice and Bob can choose freely in which setting the measurement should be performed. The setting belonging to Alice we will call a and the one belonging to Bob b . In every experimental run Alice and Bob read out the detector. We will call the result for Alice A and the one for Bob B . As already mentioned before, the possible outcomes are $A = \pm 1$ and $B = \pm 1$.

We can now write down the joint conditional probability distribution as

$$P(A, B|a, b), \tag{3.1}$$

which gives the probability for the appearance of a specific pair of outcomes

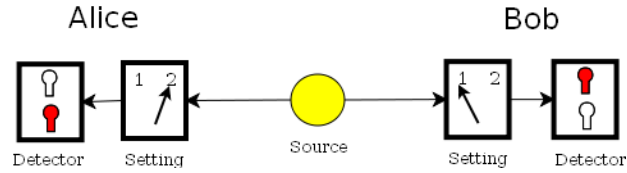


Figure 3.1: Gedanken experiment with the switches determining experimental setting, detector and source. Alice and Bob each own one experimental setting and one detector.

A and B under the condition of the chosen setting a and b . If the two results A and B are correlated one has:

$$P(A, B|a, b) \neq P(A|a)P(B|b). \quad (3.2)$$

Now we suppose that there is a so-called local hidden variable λ , that is shared by the two particles at Alice and Bob. This additional variable would allow to write the joint probability as:

$$P(A, B|a, b, \lambda) = P_1(A|a, \lambda)P_2(B|b, \lambda) \quad (3.3)$$

The average probability can then be calculated by

$$P(A, B|a, b) = \int_{\Gamma} f(\lambda)P(A, B|a, b, \lambda)d\lambda, \quad (3.4)$$

whereby $f(\lambda)$ is the probability distribution of the variable λ and Γ is the total λ space.

We will introduce now the correlation function $E(a, b)$:

$$E(a, b) = P(+, +|a, b) + P(-, -|a, b) - P(+, -|a, b) - P(-, +|a, b) \quad (3.5)$$

With 3.4 and 3.3 we get:

$$\begin{aligned} E(a, b) &= \int_{\Gamma} f(\lambda)(P(+, +|a, b, \lambda) + P(-, -|a, b, \lambda) \\ &\quad - P(+, -|a, b, \lambda) - P(-, +|a, b, \lambda))d\lambda \\ &= \int_{\Gamma} f(\lambda)((P_1(+|a, \lambda) + P_1(-|a, \lambda)) \\ &\quad (P_2(+|b, \lambda) - P_2(-|b, \lambda)))d\lambda \\ &= \int_{\Gamma} f(\lambda)\bar{A}(a, \lambda)\bar{B}(b, \lambda)d\lambda \end{aligned} \quad (3.6)$$

with $\bar{A}(a, \lambda) = (P_1(+|a, \lambda) + P_1(-|a, \lambda))$, $\bar{B}(b, \lambda) = (P_2(+|b, \lambda) - P_2(-|b, \lambda))$. Because P_1 and P_2 are probabilities, they have the property:

$$0 \leq P_i \leq 1 \quad (3.7)$$

From this follows

$$|\bar{A}(a, \lambda)| \leq 1 \quad |\bar{B}(a, \lambda)| \leq 1 \quad (3.8)$$

With 3.6 we get

$$E(a, b) \pm E(a, b') = \int_{\Gamma} f(\lambda) \bar{A}(a, \lambda) (\bar{B}(b, \lambda) \pm \bar{B}(b', \lambda)) d\lambda \quad (3.9)$$

and then from 3.8

$$|E(a, b) \pm E(a, b')| \leq \int_{\Gamma} f(\lambda) |(\bar{B}(b, \lambda) \pm \bar{B}(b', \lambda))| d\lambda \quad (3.10)$$

and

$$|E(a', b) \mp E(a', b')| \leq \int_{\Gamma} f(\lambda) |(\bar{B}(b, \lambda) \mp \bar{B}(b', \lambda))| d\lambda. \quad (3.11)$$

With 3.8 this gives us

$$|\bar{B}(b, \lambda) \pm \bar{B}(b', \lambda)| + |\bar{B}(b, \lambda) \mp \bar{B}(b', \lambda)| \leq 2. \quad (3.12)$$

Using

$$\int_{\Gamma} f(\lambda) d\lambda = 1 \quad (3.13)$$

we obtain

$$|E(a, b) \pm E(a, b')| + |E(a', b) \mp E(a', b')| \leq 2, \quad (3.14)$$

which is the Bell inequality in the CHSH form [7].

The locality is assumed by the fact that the hidden variable λ makes the separation of the probability distribution possible, which means that the outcome at Alice is totally independent of Bob's setting.

A third assumption is "free will", which is the assumption that $f(\lambda)$ does not depend on the local settings a and b .

Now, we will compare this result with the predictions of quantum mechanics. Therefore we will replace the statistical mean values $E(a, b)$ with the quantum mechanical expectation values $\langle a_i b_j \rangle$, which are defined as:

$$\langle a_i b_j \rangle = |\vec{a}_i| |\vec{b}_j| \cos(\angle a_i b_j), \quad (3.15)$$

So we get:

$$K = \langle a_1 b_1 \rangle + \langle a_2 b_1 \rangle + \langle a_2 b_2 \rangle - \langle a_1 b_2 \rangle, \quad (3.16)$$

with (3.15) and $|\vec{a}_i| = |\vec{b}_j| = 1$, we obtain:

$$K = \cos(\angle a_1 b_1) + \cos(\angle a_2 b_1) + \cos(\angle a_2 b_2) - \cos(\angle a_1 b_2) \quad (3.17)$$

Now we can imagine an experiment very similar to figure 3.1. The experiment consists of a source, two polarization filters that are turned to each other by an solid angle of 22.5° and which are turnable by 45° and two detectors that measure the incoming photons (see fig 3.2).

The source emits polarization entangled photons in the state $|\Psi\rangle = \frac{|HV\rangle + |VH\rangle}{\sqrt{2}}$

(H for the horizontal and V for the vertical polarized state) and sends one to Alice and the other one to Bob.

Upon receiving the photons, Alice and Bob can measure the polarization

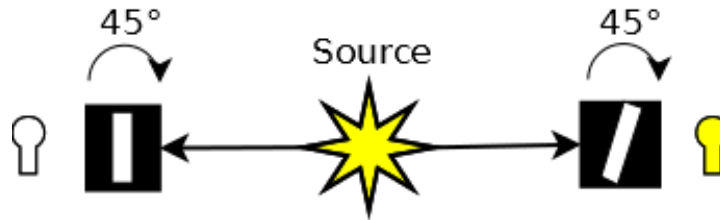


Figure 3.2: EPR experiment with photons entangled in polarization.

of the photons with their polarization filters. The directions of the measurement can be plotted on the Bloch sphere. Note that the solid angles and the angles on the Bloch sphere differ by a factor of 2 and that $|\pm 45^\circ\rangle = \frac{|H\rangle \pm |V\rangle}{\sqrt{2}}$.

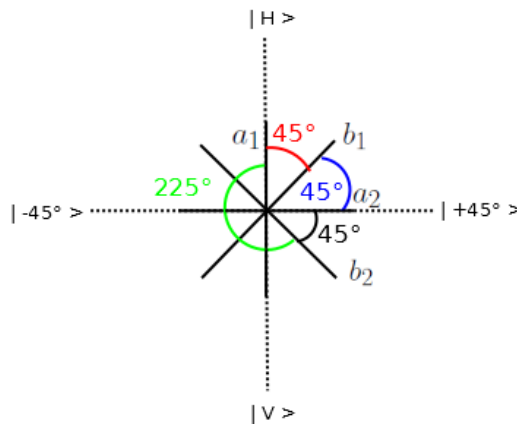


Figure 3.3: Measurement directions on the Bloch sphere.

With (3.14) we obtain:

$$\begin{aligned} \cos(45^\circ) + \cos(45^\circ) + \cos(45^\circ) - \cos(225^\circ) &= \\ &= \frac{1}{\sqrt{2}} + \frac{1}{\sqrt{2}} + \frac{1}{\sqrt{2}} - \left(-\frac{1}{\sqrt{2}}\right) = 2\sqrt{2} \end{aligned} \quad (3.18)$$

This clearly is a violation of 3.14, which means that at least one of the assumptions we have made does not hold in quantum mechanics. Violations of this kind can be found in many quantum mechanical systems. If we assume the free will assumption to hold, it means that quantum mechanics can not be explained by any local realistic theory.

3.4 Wigner inequality

Based on John Bell's inequality Eugen Wigner formulated in 1970 an inequality for two perfectly correlated particles. To derive this inequality, we will start with the Bell inequality in CHSH form (see equation 3.14), where we will replace equation 3.5 with

$$C_{nm} = P_{nm}(+; +) + P_{nm}(-; -) - P_{nm}(+; -) - P_{nm}(-; +). \quad (3.19)$$

Whereby, n is the setting at Alice and m is the setting at Bob. The settings will be chosen such that one of the possible settings at Alice and Bob is identical (the same measurement is performed).

When we assume perfect correlations between the two particles all correlation functions with $n = m$ will be 1. Using equation 3.14 this gives us:

$$C_{12} + C_{23} - C_{13} \leq 1 \quad (3.20)$$

In the local realistic case this inequality is satisfied because if two of the correlation functions are fixed the third is bounded as given by 3.20. This means if we measured e.g. the value of C_{12} and C_{23} we know the outcome of C_{13} without measuring.

For a quantum mechanical description we have to exchange the statistical expectation values with the quantum mechanical ones. This gives us:

$$K = \langle a_1 b_2 \rangle + \langle a_2 b_3 \rangle - \langle a_1 b_3 \rangle \quad (3.21)$$

We could imagine a similar experiment as described in figure 3.2, where the a_n and b_m are the directions of the measurement.

With $\langle a_n b_m \rangle = \cos \angle(a_n, b_m) = \cos \alpha_{nm}$, we get:

$$K = \cos \alpha_{12} + \cos \alpha_{23} - \cos \alpha_{13} \quad (3.22)$$

If we choose the angles to be $\alpha_{12} = 45^\circ$, $\alpha_{23} = 90^\circ$ and $\alpha_{13} = \alpha_{12} + \alpha_{23} = 135^\circ$, we end up with:

$$K = \sqrt{2} \quad (3.23)$$

Thus we obtain a violation of the Wigner inequality. Again, we get a contradiction between the predictions of the classical world view and quantum mechanics.

3.5 Leggett-Garg inequality

Until now, we have discussed inequalities with two particles. In general, it is also possible to extend Bell inequalities to more particles. These particles will still be treated separately though. The question arises if similar inequalities can be found also for the case where particles strongly interact, as e.g. in a solid-state system, such that one has access to collective degrees of freedom only and not to single particles. Then, the entire ensemble of particles behave as a single quantum system. In 1985, Anthony James Leggett and Anupam Garg found an inequality that exactly addresses this problem [8].

They derived the inequalities from the so-called macrorealism. Leggett summarized the assumptions behind this notion as follows [9]:

Macrorealism per se.: "A macroscopic object which has available to it two or more macroscopically distinct states is at any given time in a definite one of those states"

Non-invasive measurability: "It is possible in principle to determine which of these states the system is in without any effect on

the state itself or on the subsequent system dynamics.”

Induction: ”The properties of ensembles are determined exclusively by initial conditions (and in particular not by final conditions).”

Consider an observable Q that has two outcomes $+1$ or -1 when measured. In the first set of runs, measurements take place only at t_1 and t_2 , in the second set of runs only measurements are conducted at t_2 and t_3 and in the third only measurements at t_1 and t_3 are performed, whereby ($0 \leq t_1 < t_2 < t_3$). Between the measurements the system is time evolved under the influence of a Hamiltonian. For each measurement we get an outcome $Q(t_i)$, from which we can calculate the temporal correlation function

$$\begin{aligned} C_{ij} &= \langle Q(t_i)Q(t_j) \rangle \\ &= P_i(+1)P_{ji}(+1|+1) + P_i(-1)P_{ji}(-1|-1) \\ &\quad - P_i(+1)P_{ji}(-1|+1) - P_i(-1)P_{ji}(+1|-1), \end{aligned} \quad (3.24)$$

whereby $P_i(Q(t_i))$ are the probabilities for a specific outcome at time t_i and $P_{ji}(Q(t_j)|Q(t_i))$ are the conditional probabilities to obtain at time t_j given the outcome obtained at t_i . The Wigner type Leggett-Garg inequality can then be written as

$$K = C_{12} + C_{23} - C_{13} \leq 1, \quad (3.25)$$

which has to be fulfilled by any macrorealistic theory. Here, K is called the Wigner expression.

To find out if quantum mechanics obeys or violates this inequality, we again insert the quantum mechanical expectation values. Using 2.11 and 2.31 we get:

$$\langle \psi(t_i) | U(t_j - t_i) | \psi_{t_i} \rangle = \cos \omega \Delta t_{ij}, \quad (3.26)$$

with ω the frequency of the rotation. This gives us:

$$K = \cos \omega \Delta t_{12} + \cos \omega \Delta t_{23} - \cos \omega \Delta t_{13} \quad (3.27)$$

As seen in 3.4 this can violate the above mentioned inequality. Consequently, we can see that quantum mechanics violates macrorealism.

3.6 Experimental violation of Bell type inequalities

The theoretical discrepancy between quantum mechanics and classical physics was a strongly discussed problem for many years. In 1967, C. A. Kocher and Eugene Commins discovered that calcium atoms emit under certain circumstances correlated photon pairs [10]. Through this discovery, the experimental examination became possible. In 1972 Stuart Freedman and John Clauser were able to show the violation of Bell type inequalities using

correlated photon pairs produced by calcium atoms [11].

Since then, many experiments validated the predictions of quantum mechanics. Moreover, experiments with other inequalities as well as "all-versus-nothing" arguments that do not involve inequalities, for example the validation of quantum mechanical predictions using so-called GHZ states. These states were predicted by D. M. Greenberger, M. A. Horne, and A. Zeilinger in 1989.

All these experiments have confirmed the predictions of quantum mechanics and ruled out local hidden variable theories. Today, it is the accepted opinion that the effects of quantum mechanics can not be explained by local realistic theories. The nature of these non-local-realistic effects is still not totally understood and is an interesting field of scientific investigation.

4 Granularity

In quantum mechanics the measurement process is of great importance, as we have seen in chapter 3. Especially in the Leggett-Garg inequality, we saw that the non-invasive measureability is an important feature for the emergence of classicality. This outstanding role of the measurement process in quantum mechanics makes it necessary to reconsider our understanding of measurements.

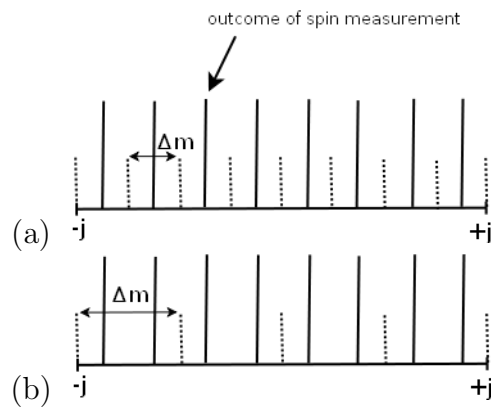


Figure 4.1: The macroscopic states with the outcome m in a sharp measurement (black lines) and the measurement precision Δm for (a) a fine grained measurement and (b) a coarse grained measurement.

In quantum mechanics the granularity can be seen as the measurement precision in comparison to the distance of neighboring states. A finer graining would resolve the individual states of the system, a coarser graining would average over neighboring states (see fig. 4.1). In the case of coarse grained measurements this would mean that states that are part of one graining cannot be distinguished in the measurement.

Not just the size of the granularity can be an important factor, also the shape of the granularity is of huge importance. Here, with the shape is meant, that it is possible to choose the coarse graining such that states that are not neighboring are indistinguishable. In the next chapter I will introduce such a coarse graining.

As in quantum mechanics the measurement process is very important the question is how the granularity of quantum mechanical measurements can effect quantum states.

5 The Wigner-type Leggett-Garg inequality under coarse-grained measurements

As seen in section 3.2, 3.4 and 3.5, Bell type inequalities can distinguish between quantum-mechanical states and those that can be understood classically. These inequalities draw a strict boarder between these two theories. The question is now if and how transitions between the quantum and the classical world can happen.

As Johannes Kofler and Časlav Brukner showed [1], macroscopic spin systems can be understood quantum mechanically, even if they appear classical when the resolution of the distinguishable eigenvalues m in a spin projection measurement is given by $\Delta m \gg \sqrt{j}$, where j is the total spin length. In order to show the quantum-mechanical features of the systems, they used the projectors $P_{\pm} = \frac{1}{2}(\mathbb{1} \pm \hat{Q})$, where $Q = \sum_{m=-j}^j (-1)^{j-m} |m\rangle\langle m|$ defines the parity measurement. Note that this measurement is a coarse grained measurement because it assigns always the next-but-one state to the same projector (see fig. 5.1).

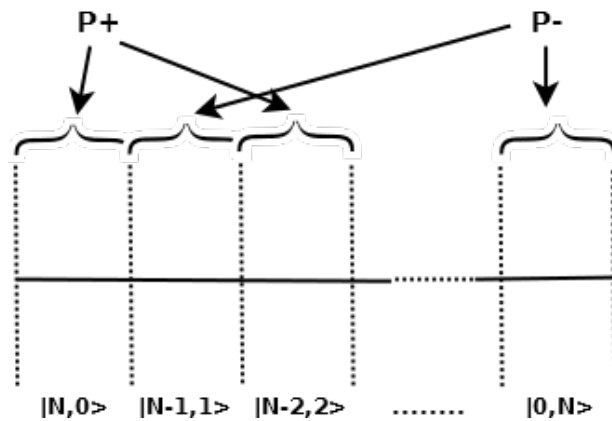


Figure 5.1: Measurement under parity coarse graining.

By using the parity measurement they were able to show that the Leggett-Garg inequality is violated for arbitrary high-dimensional systems. In the case of composite systems, this illustrates that even huge particle clouds can behave quantum mechanically under very particular coarse grained measurements. Furthermore, they showed that under sharp POVM any non-trivial Hamiltonian can lead to a violation of the Wigner type Leggett-Garg inequality. [12]

On the other hand, Kofler and Brukner showed that states that under sharp measurement behave quantum mechanically can appear classically when fuzzy measurements are performed [1] [12]. Under fuzzy measurements in

which neighboring states are joined into slots, any macroscopic spin state can appear as a classical mixture. [12]

The transition between the quantum mechanically behavior under parity measurements and the classically interpretable results of fuzzy measurements is the object of interest of this thesis.

5.1 Calculation of the Wigner expression K

In order to calculate the Wigner expression K for the Wigner type Leggett-Garg inequality we first choose an initial state. For reasons of simplicity I chose the initial state to be the fully polarized state $|\uparrow\rangle^{\otimes N}$, on which also the first measurement is conducted. For this measurement, we will project the state in the reduced basis on the directions $+$ and $-$. We will call the corresponding projectors P_+ and P_- . These projectors are constructed by assigning the different states in the reduced basis to P_+ or P_- . One possibility for this assignment is to choose randomly which state belongs to which direction (see section 5.3). Another possibility is to create slots in which neighboring states can be bundled (see section 5.2). Under the assumption that $|N, 0\rangle$ is always assigned to P_+ , the initial state will not change during the measurement and can now be time evolved by the Hamiltonian $\hat{H} = \hat{J}^2/2I + \omega J_y$, whereby ω is the spin precision frequency, J_y is the y-component of the total spin vector \hat{J} and I is the moment of inertia. In this case $\hat{J}^2/2I$ commutes with the spin projection, so only ωJ_y contributes to the time evolution. With 2.11 and 2.30, we end up with the time evolution given by $U(t) = e^{-i\omega t J_y}$, where $J_i = \sum_{k=1}^N \frac{\sigma_{ik}}{2}$, with $i = x, y, z$. Then we can write the time evolution as $U(t) = U(t)_k^{\otimes N}$, whereby k numbers the individual particles and $U(t)_k = -i\frac{\omega t}{2}\sigma_y$. The overall time evolution is now calculated as the time evolution of the subsystems, as discussed in 2.3. The state in the spin basis after the first time evolution is then given by:

$$|\psi_{12}\rangle = (\cos \omega t |\uparrow\rangle + \sin \omega t |\downarrow\rangle)^{\otimes N}. \quad (5.1)$$

The next step is now to conduct the second measurement on our system. After applying the projectors to the evolved state we end up with the two probabilities $P_{21}(+1|+1)$ and $P_{21}(-1|+1)$ to measure the system being in state $+$ or $-$. If we just include projections where projector onto $|N, 0\rangle$ is part of P_+ and projector onto $|0, N\rangle$ of P_- , the probability $P_1(-1)$ is zero, because we started in the state in which all spins are "up". After the measurement the projected state will be either $|\psi_{12}^+\rangle$ or $|\psi_{12}^-\rangle$ depending on which outcome has been observed. With the measured probabilities, the correlation function

$$C_{12} = P_1(+1)P_{21}(+1|+1) - P_1(+1)P_{21}(-1|+1) \quad (5.2)$$

can be calculated (see equation 3.24). Here, $P_1(+1) = 1$ because the state $|N, 0\rangle$ is always assigned to P_+ . Under the assumption that the total rotation angle ωt of each time evolution is for each time step the same, we can also evaluate C_{13} by just adding a factor 2 to the angle of rotation.

After the second measurement, the reduced states have to be converted

back into the spin basis to calculate the second time evolution. In order to do so, we again have to calculate the time evolution of every individual spin as explained in section 2.3. The states after this second time evolution are given by $|\psi_{23}^+\rangle$ and $|\psi_{23}^-\rangle$. These states have to be reconverted from the spin states to the reduced states to conduct the last measurement. This measurement gives us the four conditional probabilities $P_{32}(+1|+1)$, $P_{32}(-1|-1)$, $P_{32}(-1|+1)$ and $P_{32}(+1|-1)$. And with $P_2(+1) = P_{21}(+1|+1)$ and $P_2(-1) = P_{21}(-1|+1)$, we are able to calculate the correlation function C_{23} and establish the formula for the Wigner expression K . After that, this formula can be maximized by varying the angle of rotation ωt to see if the inequality is violated under any angle.

In this approach it is necessary to change the basis of the state from the spin representation to the reduced basis to apply the projective measurement. A much more elegant way to apply the time evolution would be to perform it directly in the reduced basis. The problem is that it is hard to find an expression for general particle numbers that generate the changes of the time evolution for different states. All tries of mine to do so failed. In further investigations, it would be very helpful to find such an expression.

5.2 Projective Slot Measurement (PSM)

One possibility to implement coarse grained measurements, as explained above, is the Projective Slot Measurement (PSM). In PSM, neighboring states are bundled together in one slot of length L and the even slots are assigned to the results $+1$, and odd to -1 . (see figure 5.2).

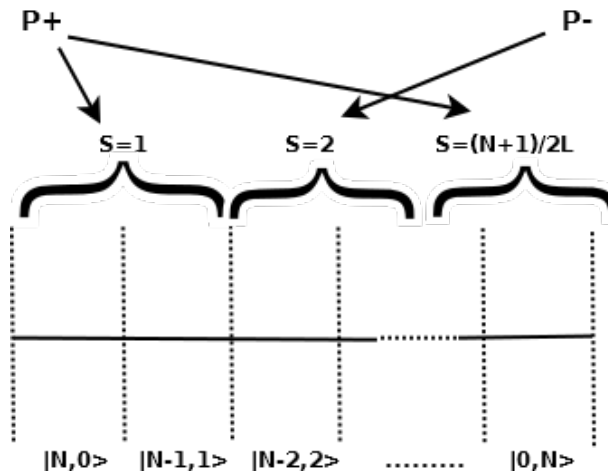


Figure 5.2: The states are bundled into slots (in this case with length $L=2$) and then projected accordingly onto $P+$ and $P-$.

The length of the slot (number of neighboring states per slot) can be chosen freely, from one state per slot (parity measurement) to half of the states ($N/2$) per slot (semi classical measurement). The projectors P_+ and P_- can then be written as

$$P_+ = \sum_{s=1}^x \sum_{r=0}^y |(N+1 - (2s-1)L + r)_{\text{up}}, ((2s-1)L - r - 1)_{\text{down}}\rangle \cdot \langle (N+1 - (2s-1)L + r)_{\text{up}}, ((2s-1)L - r - 1)_{\text{down}}|. \quad (5.3)$$

and

$$P_- = \sum_{s=1}^x \sum_{r=0}^y |(N+1 - 2sL + r)_{\text{up}}, (2sL - r - 1)_{\text{down}}\rangle \cdot \langle (N+1 - 2sL + r)_{\text{up}}, (2sL - r - 1)_{\text{down}}|. \quad (5.4)$$

With L the length of the slots, $x = \frac{N+1}{2L}$ the number of slots and $y = L-1$. To have x integer, we assume odd particle numbers N and also choose L such that x remains integer.

5.3 Random Projection Measurement (RPM)

A second possibility to assign a state to the projection direction is by doing it randomly (see fig. 5.3).

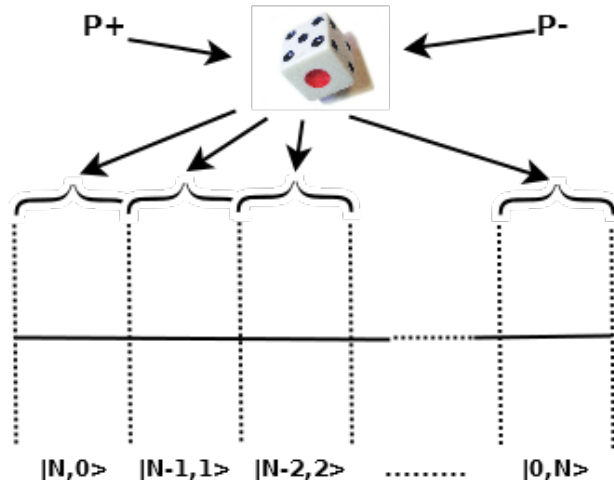


Figure 5.3: The projection direction for each state is chosen randomly.

In this case, the projectors are given by:

$$P_+ = \sum_{h=1}^{\frac{N+1}{2}} |(N+1 - v[h])_{\text{up}}, (v[h] - 1)_{\text{down}}\rangle \cdot \langle (N+1 - v[h])_{\text{up}}, (v[h] - 1)_{\text{down}}|. \quad (5.5)$$

and

$$P_- = \sum_{i=\frac{N+1}{2}+1}^{N+1} |(N+1-v[i])_{\text{up}}, (v[i]-1)_{\text{down}}\rangle \cdot \langle (N+1-v[i])_{\text{up}}, (v[i]-1)_{\text{down}}| \quad (5.6)$$

Whereby v is a random list of the numbers 1 to $N+1$.

The RPM was conducted in the simulation to find out if there are any combinations for P_+ and P_- that have a higher or lower violation of the Leggett-Garg inequality, than it is possible in measurements with PSM.

5.4 Numerical solution

In order to simulate the violation of the Wigner type Leggett-Garg inequality I used Mathematica and the QuantumNotation package from José Luis Gómez-Muñoz and Francisco Delgado.

The task was to write a code that simulates the Wigner expression K of the inequality for a large number of particles with the angle of rotation as a variable. In sections 5.1, 5.2 and 5.3, I already showed how to calculate the inequality and how the projectors can be implemented. The remaining task was to find a way to implement the time evolution in the simulation. The two main difficulties were the conversion and back conversion from the spin to the reduced states and the time evolution itself.

In the computational solution we start with the spin state

$|\psi\rangle = \bigotimes_{a=1}^n (\text{Cos}[w] \cdot |0_{\hat{a}}\rangle + \text{Sin}[w] \cdot |1_{\hat{a}}\rangle)$, so after the first time evolution.

Note that in this notation the $|0_{\hat{i}}\rangle$ are the $|\uparrow\rangle$ and the $|1_{\hat{i}}\rangle$ are the $|\downarrow\rangle$. For the conversion from the spin states to the reduced states, I used the following For-loop:

$$\begin{aligned} &\text{For}[j = 0, j \leq n, j++, \\ &\text{If}[j < 1, |\phi\rangle = |\phi\rangle, |\phi\rangle = |1_{\hat{j}}\rangle \cdot \langle 0_{\hat{j}}| \cdot |\phi\rangle]; \\ &|\psi_{kl}\rangle = |\psi_{kl}\rangle + \sqrt{\text{Binomial}[n, j]} |j_{\text{down}}, (n-j)_{\text{up}}\rangle \cdot (|\phi\rangle)^\dagger \cdot |\psi\rangle \end{aligned} \quad (5.7)$$

Whereby $|\phi\rangle = \bigotimes_{i=1}^n |0_{\hat{i}}\rangle$ and $|\psi\rangle$ are the spin states and the index kl defines the time interval. This For-loop can be used because the prefactors for all terms of the spin states belonging to the same reduced state are equal.

The reconversion from the reduced states to the spin states is then implemented by using:

$$\begin{aligned} &\text{For}[j = -n, -n \leq j \leq n, j++, \\ &\text{If}[\text{Element}\left[\left(\frac{j}{2} + \frac{1}{2}\right), \text{Integers}\right], \\ &|\psi'_{xy}\rangle = |\psi'_{xy}\rangle + 1 / \sqrt{\text{Binomial}[n, (j+n)/2]} \cdot \\ &\text{With}[\{m = j\}, \text{Sum}[\\ &\text{If}[\text{DigitSum}[a] == m, \bigotimes_{k=0}^{n-1} |(-\text{BitGet}[a, k] + 1)_{k\hat{+}1}\rangle, 0], \\ &\{a, 0, 2^n - 1\}]] \cdot \langle (n - (j+n)/2)_{\text{down}}, ((j+n)/2)_{\text{up}}| \cdot |\phi_{xy}\rangle] \end{aligned} \quad (5.8)$$

Here, the With-loop gives the sum over all permutations of the spin state for a given reduced state $|\phi_{xy}\rangle$, where the index xy defines the time interval. The large computational complexity of the time evolution was a big problem. The QuantumNotation package reaches its limits, using an up-to-date PC, at particle numbers of 5-7 (for higher particle numbers the evaluation time is too long). To increase the speed of the evaluation, I used the matrix representation for the spin states to compute the time evolution. This speeds up the code and a computation with particle numbers up to $N=11$ were possible. To change between the Dirac notation and the matrix representation, I used the DiractoMatrix and MatrixtoDirac functions of the QuantumNotation package.

In retrospect, it would have been better to write the code from the beginning in matrix representation. This would have resulted in a higher speed because less conversions would have been necessary. One problem in matrix representation though is the representation of the projectors in the reduced states. In future codes, this problem can be solved by using the spin representation for the projectors. For now, a particle number of $N = 11$ is sufficient and the refinement of the code can be done for future simulations. The present code can be used for arbitrary particle numbers. The different measurements, as e.g. PSM and RPM, can be implemented by just exchanging the construction of the projectors.

For the analysis, I used the NMaximize function of Mathematica which gives the maximal violation for the inequality.

5.5 Results

PSM

For PSM I used the particle number $N = 11$ and a slot length of $L = 1, 2, 3, 6$. I did not use the value $L = 4$ because it would lead to an uneven assignment of the states to the projection operators.

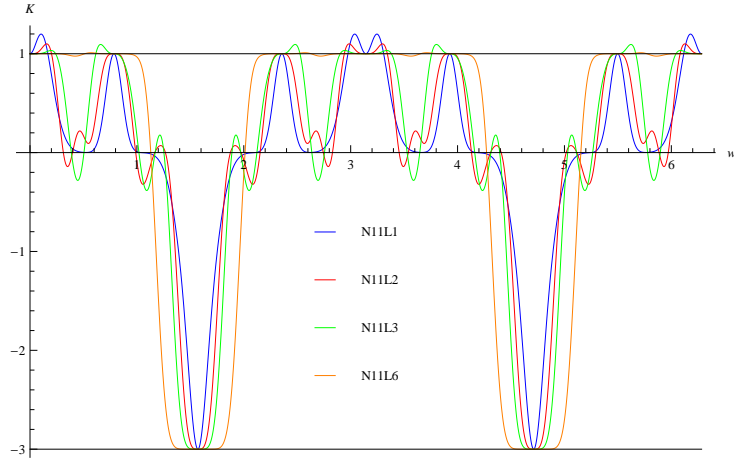


Figure 5.4: Values of the temporal correlation function depending on the angle of rotation for $N = 11$ and $L = 1$ in blue, $L = 2$ in red, $L = 3$ in green and $L = 6$ in orange.

In figure 5.4, one can see the value of the Wigner expression maximized over the rotation angle for different values of L . The maximal values of K with the corresponding angle $w = \omega t$ are then:

L	K	w
1	1.1986	0.1038
2	1.0996	0.1560
3	1.0938	0.6607
6	1.0102	0.5689

Table 5.1: The maximal values of K with the corresponding angle w

As expected the value decreases from a maximum of 1.1986 (at global maximum) for the parity measurement to a minimum of 1.0102 (at global maximum) for the semiclassical measurement. Initially, a dropping of the value to 1 was expected, so that no violation of the inequality is measured in the semiclassical case. This is clearly not observed. One explanation for this behavior could be the use of projective measurements instead of POVM. The rather sharp projective measurements could lead to a disturbance of the state. One indication for this hypothesis is also that, starting from $L = 3$, the dominant violation of the inequality is at a different angle than before. This effect should be studied more in detail to make better predictions.

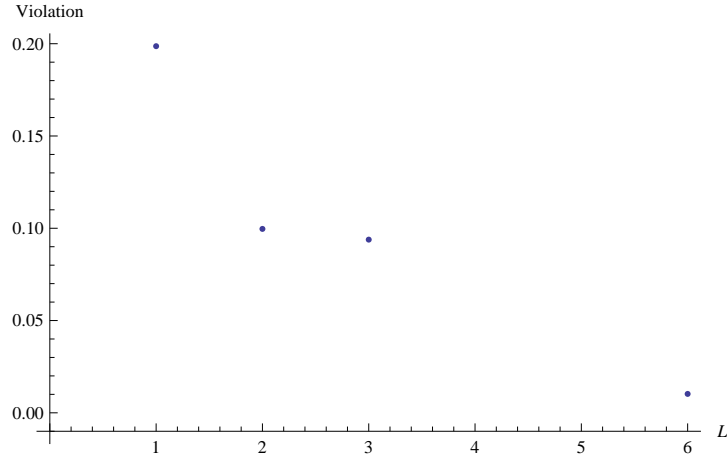


Figure 5.5: Values of the violation for the global maximum of the Wigner expression K for different L.

In figure 5.5, we can clearly see that the violation of the Wigner type Leggett-Garg inequality is decreasing for larger slot sizes, as expected. This means, that under these circumstances the classical description of a state arises out of the fact that single quantum mechanical states cannot be resolved.

RPM

Using the RPM projectors, I produced large output files. I selected these lists and give below a list outcomes. Note that due to the construction of the code only outcomes with the total polarized state $|N, 0\rangle$ projected onto + and $|0, N\rangle$ projected onto - could be used. The goal was to find out if there are projectors for which the Wigner type inequality is stronger violated than for PSM.

For a particle number of $N = 11$, we end up with 665280 possible combinations for the projectors. Due to the assignment of $|N, 0\rangle$ to P_+ and $|0, N\rangle$ to P_- , only 55440 could be used for analysis. I used a much smaller number of combinations, such that the following results can just be seen as a small selection and it is even possible that there are projectors for which the value of K might be larger or smaller.

It seems that there are many possibilities for choices of projectors such that the violation of the Wigner type Leggett-Garg inequality is larger than in the case of parity measurement. In table 5.2, I give a selection of projectors which lead to a higher violation of the inequality.

The most common values of K that are higher than the value for the parity measurement were between 1.3 and 1.4. The quantum mechanical bound of the inequality of $K = 1.5$ was not reached in the available data.

These results are very interesting because one would expect that the parity measurement leads to the highest violation of the inequality.

Violations lower than those of the semi classical measurement were very rare. In fact, I found only one set of projectors in my data that lead to a lower violation. The projector P_+ of this set is given by

K	p	Plot of K over w
1.19867	0,2,4,7,8,9	
1.2178	0,1,2,3,5,6	
1.25287	0,1,2,3,4,8	
1.31029	0,3,5,8,9,10	
1.38973	0,4,6,8,9,10	
1.41922	0,5,6,7,8,9	
1.42713	0,6,7,8,9,10	

Table 5.2: List of the values of K , with the reduced states given by the values of the numbers of particles with spin down p that are projected onto P_+ and the plot for the values of K over the angle w .

$$\begin{aligned}
P_+ = & |11_{\hat{u}p}, 0_{\hat{d}wn}\rangle \cdot \langle \dots | + |10_{\hat{u}p}, 1_{\hat{d}wn}\rangle \cdot \langle \dots | + |9_{\hat{u}p}, 2_{\hat{d}wn}\rangle \cdot \langle \dots | \\
& + |8_{\hat{u}p}, 3_{\hat{d}wn}\rangle \cdot \langle \dots | + |5_{\hat{u}p}, 6_{\hat{d}wn}\rangle \cdot \langle \dots | + |2_{\hat{u}p}, 9_{\hat{d}wn}\rangle \cdot \langle \dots |
\end{aligned} \tag{5.9}$$

and leads to the value $K = 1.00649$. In figure 5.6 we can see the value of K over the rotation angle.

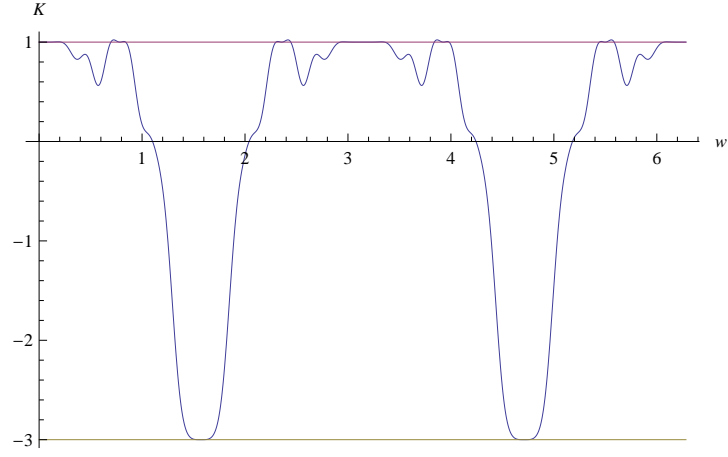


Figure 5.6: The value of K over the rotation angle of the time evolution w for the minimum violation.

6 State disturbance due to coarse-grained measurements

As we have already seen in section 2.2, the quantum mechanical measurement concept is fundamentally different from the classical concept of measurements. In quantum mechanics, a measurement leads to different states before and after the measurement, such that the assumption of a non-invasive measurement is clearly refuted. The question is then, which effect do coarse grained measurements have on the state of a quantum system.

As Asher Peres showed, a quantum mechanical systems undergoes the less disturbance, the more fuzzy a measurement is (see [13], page 398). To show this he used the macroscopic spin state of a particle ensemble, which at the beginning was in the full polarized state $|\psi_1 = |z+\rangle^{\otimes N}$. Then, the state is rotated around the x-axis by $\pi/2$. If now a sharp measurement in z-direction is executed we end up with the probability distribution shown in figure 6.1.

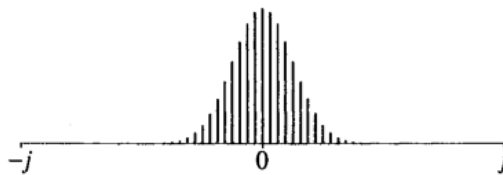


Figure 6.1: Expected probability distribution for a measurement of J_z after a rotation of $\pi/2$ around the x-axis, with $j=32$. (figure taken from [13])

If we turned this state by another $\pi/2$ without measuring it, we would end up with the total polarized state $|\psi_2 = |z-\rangle^{\otimes N}$. The question is now, how the state after the second rotation would look like if a fuzzy measurement was executed after the first rotation.

As we can see in figure 6.2, the outcome of the second measurement depends on the fuzziness of the first measurement. A sharp measurement totally destroys the state, so that the second measurement gives a mixture of all states and not the expected state $|\psi_2 = |z-\rangle^{\otimes N}$. The more fuzzy the measurement gets, the more similar the state becomes to the expected state without disturbing measurement. If these results can be reconstructed by using PSM and RPM is the subject of the following contemplation.

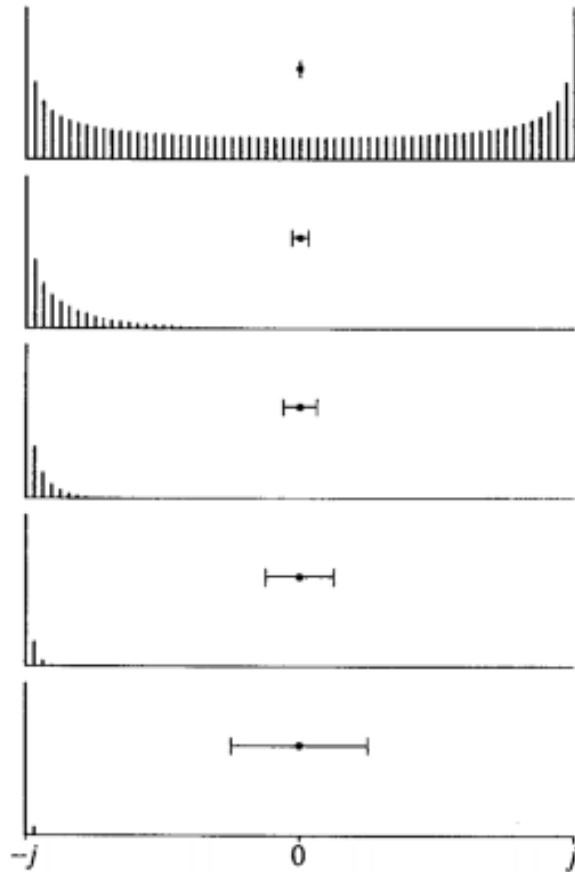


Figure 6.2: Expected probability distributions for a second measurement of J_z , after one more rotation by $\pi/2$. The results depend on the Δm of the meter which performed the first measurement. From top to bottom, this Δm (shown as a horizontal error bar) is 0, 1, 2, 4, and 8. Different vertical scales are used in the various diagrams, for better visibility. In each diagram, the sum of lengths of the vertical bars is 1, by definition. (figure and caption taken from [13])

6.1 Numerical solution

For the computation of the state disturbance, proposed by Peres, I used a modified version of the code explained in section 5.4. Again we will start the code after the first time evolution with the state

$|\psi\rangle = \bigotimes_{a=1}^n (\text{Cos}[w] \cdot |0_a\rangle + \text{Sin}[w] \cdot |1_a\rangle)$. I will again simulate the outcome depending on the angle of rotation and insert later $w = \pi/4$ because otherwise the numerical calculation lead to errors and incorrect solutions due to rounding errors.

For the coarse grained measurement I chose PSM and selected projectors of RPM. Since the outcomes for P_+ and P_- are the same, I decided to present only the outcomes for P_+ . For the state evolution after the coarse grained measurement I use the time evolution as explained in chapter 5. The time evolved state is then measured sharply along z -direction and the resulting probability distribution is plotted.

6.2 Results

PSM

To clarify how the state looks like after the first rotation, I made a sharp measurement of the state after the first time evolution in z -direction. As one can see in figure 6.3, the resulting probability distribution corresponds to the probability distribution in figure 6.1.

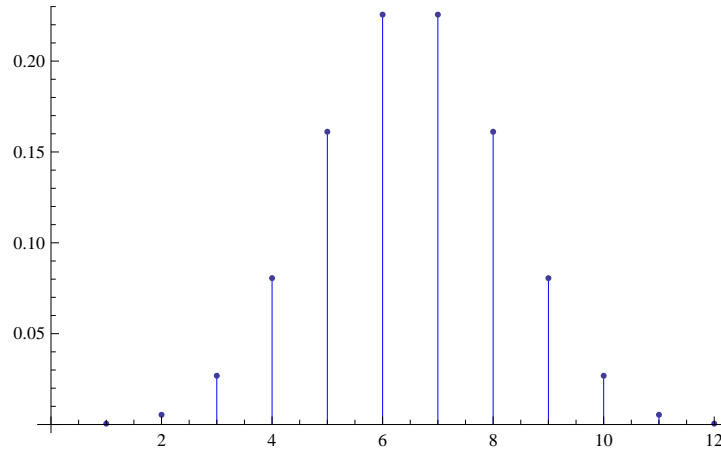


Figure 6.3: Sharp measurement after the first rotation by $\pi/2$. With the total polarized state $|\uparrow\rangle^{\otimes N}$ on the right side of the coordinate system.

If we execute now the PSM with the slot length $L = 1, 2, 3, 6$ and turn the state by another $\pi/2$, we obtain after the sharp measurement, the probability distributions, as shown in figure 6.4.

If we compare the sharpest of the fuzzy measurements in figure 6.2 with the sharpest of our coarse grained measurements, the parity measurement, one can see that we get the two total polarized states instead of a superposition between all states. For larger and larger L one can see that the probability distribution forms closer and closer to the value that would be expected

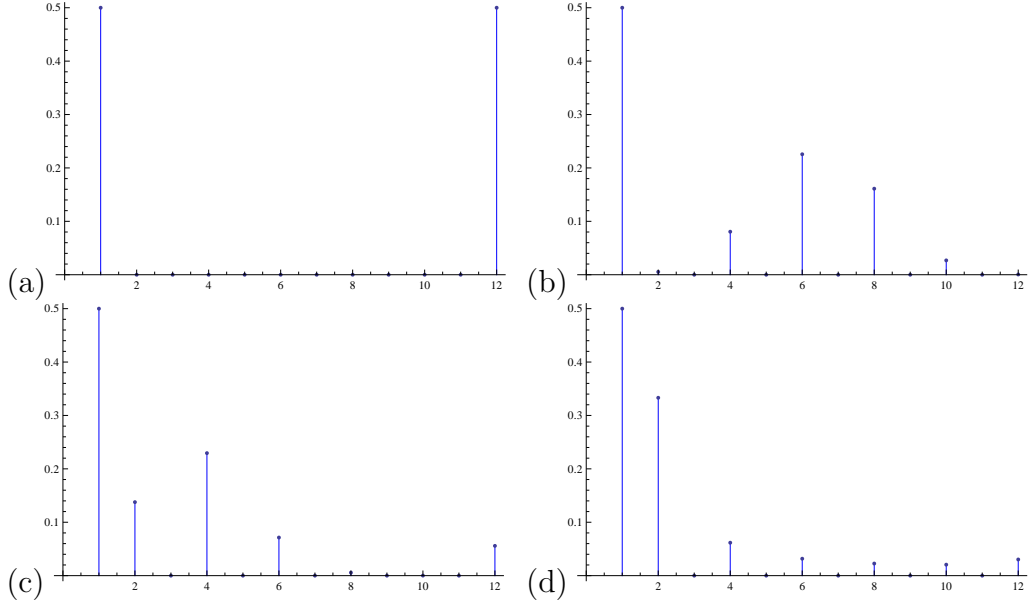


Figure 6.4: Probability distribution of the coarse grain measured state after the second rotation with (a) $L = 1$, (b) $L = 2$, (c) $L = 3$ and (d) $L = 6$. With $N-p+1$ on the x -axis.

without any measurement. For $L = 6$, the semi classical measurement, the probability distribution is around the fully polarized state, but unlike in the simulation of Peres, I never measured the state $|\downarrow\rangle^{\otimes N}$ with probability 1. This corresponds with the result that the violation of the Wigner type Leggett-Garg inequality is not vanishing for the semi classical measurement and may occur, as mentioned before, because I used projective measurements instead of POVM and have a small number of particles.

I was able to show that the semi classical measurement gives outcomes close to the value one would expect when no disturbing measurement is performed, while the parity measurement leads to a higher state disturbance. The smaller the value of L , the bigger the disturbance of the initial state, which corresponds to the considerations of Peres.

Analytical results for the outcomes of the parity measurement

The time evolution for the rotation around the y -axis of $\pi/2$ is given by

$$\hat{U}(t) = e^{-i\frac{\pi}{2}\hat{J}_y}. \quad (6.1)$$

The projectors for the parity measurement are:

$$\hat{P}_{\pm} = \frac{\mathbb{1} \pm \hat{Q}}{2}. \quad (6.2)$$

Where the parity measurement operator is given by (see chapter 5):

$$\hat{Q} = e^{i\pi(j-\hat{J}_z)}. \quad (6.3)$$

The joint operator for the two time evolutions and the parity measurement is then

$$\hat{U}(t) \cdot \hat{Q} \cdot \hat{U}(t) = \frac{1}{2} e^{-i\frac{\pi}{2}\hat{J}_y} \cdot e^{-i\frac{\pi}{2}\hat{J}_y} \pm \frac{1}{2} e^{-i\frac{\pi}{2}\hat{J}_y} e^{-i\pi\hat{J}_z} e^{-i\frac{\pi}{2}\hat{J}_y}. \quad (6.4)$$

Whereby I neglected the j -term, because it will just give an additional phase. Using 2.30, we obtain:

$$\begin{aligned} \hat{U}(t) \cdot \hat{Q} \cdot \hat{U}(t) &= \frac{1}{2} (\mathbb{1} \cos \frac{\pi}{4} - i\hat{\sigma}_y \sin \frac{\pi}{4})^{\otimes N} \cdot (\mathbb{1} \cos \frac{\pi}{4} - i\hat{\sigma}_y \sin \frac{\pi}{4})^{\otimes N} \pm \\ &\frac{1}{2} (\mathbb{1} \cos \frac{\pi}{4} - i\hat{\sigma}_y \sin \frac{\pi}{4})^{\otimes N} \cdot (\mathbb{1} \cos \frac{\pi}{2} - i\hat{\sigma}_z \sin \frac{\pi}{2})^{\otimes N} \cdot (\mathbb{1} \cos \frac{\pi}{4} - i\hat{\sigma}_y \sin \frac{\pi}{4})^{\otimes N} \end{aligned}$$

With the mixed product property of the Kronecker product, this gives

$$\begin{aligned} \hat{U}(t) \cdot \hat{Q} \cdot \hat{U}(t) &= \frac{1}{2} ((\mathbb{1} \frac{1}{\sqrt{2}} - i\hat{\sigma}_y \frac{1}{\sqrt{2}}) \cdot (\mathbb{1} \frac{1}{\sqrt{2}} - i\hat{\sigma}_y \frac{1}{\sqrt{2}}))^{\otimes N} \pm \\ &\frac{1}{2} ((\mathbb{1} \frac{1}{\sqrt{2}} - i\hat{\sigma}_y \frac{1}{\sqrt{2}}) \cdot (-i\hat{\sigma}_z) \cdot (\mathbb{1} \frac{1}{\sqrt{2}} - i\hat{\sigma}_y \frac{1}{\sqrt{2}}))^{\otimes N} \end{aligned}$$

And we get:

$$\hat{U}(t) \cdot \hat{Q} \cdot \hat{U}(t) = \frac{1}{2} (-i\hat{\sigma}_y)^{\otimes N} \pm \frac{1}{2} (-i\hat{\sigma}_z)^{\otimes N} \quad (6.5)$$

If we apply this operator to the total polarized state $|N, 0\rangle = |\uparrow\rangle^{\otimes N}$, we end up with:

$$\frac{1}{2} ((-i\hat{\sigma}_y)^{\otimes N} \pm (-i\hat{\sigma}_z)^{\otimes N}) \cdot |\uparrow\rangle^{\otimes N} = \frac{1}{\sqrt{2}} (|\downarrow\rangle^{\otimes N} \pm (-i)^N |\uparrow\rangle^{\otimes N}) \quad (6.6)$$

Whereby I have already inserted the new normalization factor in the last step. This is the measured even superposition of the two total polarized states.

RPM

Animated by the surprising outcome in subsection 5.5, I wanted to see if the projectors that lead to a stronger or weaker violation of the inequality then PSM will also disturb a state more respectively less. For this purpose I used again the scheme of Peres and just replaced the PSM by the corresponding RPM projectors.

First I chose the projectors with the highest violation of the Winger-type Legget-Garg inequality out of chart 5.2. As one can see in figures 6.5 the projectors for a violation of 0.41922 lead to a different probability distribution for P_+ and P_- . The probability distribution is close to the expected value without any measurement but the probability for the exact expected state is lower than in the semiclassical case.

More surprising is the resulting probability distribution for the projectors that give a violation of 0.42713. This probability distribution is similar to the distribution given by the semiclassical measurement which is unexpected because naively thinking one would expect that a higher state disturbance would also lead to a higher violation of the inequality.

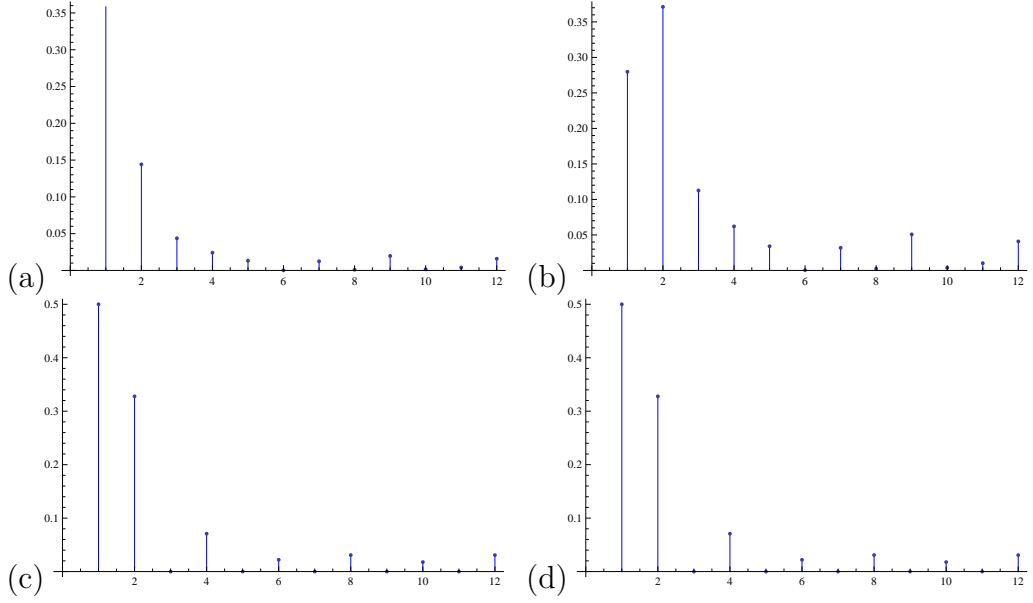


Figure 6.5: Probability distribution of the coarse grain measured state after the second rotation for (a) P_+ given a violation of 0.41922, (b) P_- given a violation of 0.41922, (c) P_+ given a violation of 0.42713, (d) P_- given a violation of 0.42713.

In figure 6.6 we can see the state disturbance for the projector which leads to a violation lower than for the semiclassical case. Very interesting here is that the state disturbance under this projector seems to be higher than the state disturbance of the parity measurement. There is also a slight difference between the probability distribution for P_+ and P_- .

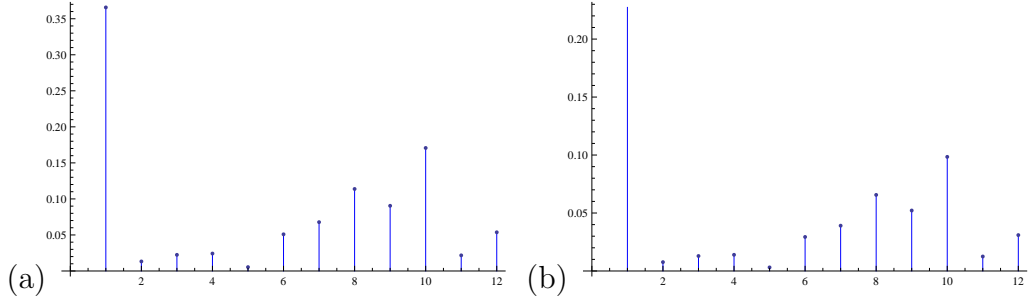


Figure 6.6: Probability distribution of the coarse grain measured state after the second rotation for (a) P_+ given a violation of 0.00649, (b) P_- given a violation of 0.00649.

These results indicate that in some cases the violation of the Leggett-Garg inequality and the state disturbance measurement proposed by Peres are not equivalent. The reasons for this behavior are not clear yet and need to be investigated more in detail.

7 Example for an implementation of coarse grained measurements in experiments

I will now present an experiment proposed by A. Kuzmich, N. P. Bigelow and L. Mandel in 1998 [14] and developed by Andres Sørensen and Klaus Mølmer [15]. In these papers, a scheme how atomic spins can be measured without destroying their spin state is presented, using the so-called Quantum Non-Demolition (QND) measurements.

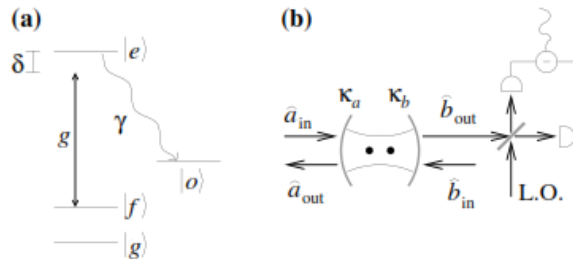


Figure 7.1: (a) Energy levels of atoms with ground state $|f\rangle$ and $|g\rangle$. The cavity couples the state $|f\rangle$ to the excited state $|e\rangle$ with the coupling strength g and detuning δ . $|e\rangle$ decays to $|o\rangle$ with the decay rate γ . (b) Scheme of the experimental realization with two atoms in a cavity. (Figure taken from [15])

In this scheme, a large number of spin particles (atoms) as well as a large number of probe particles (photons) is used. The spin particles are trapped inside an optical cavity. The photons are sent into the cavity and can interact with the atomic spin states (see figure 7.1). In our case $|g\rangle = |\downarrow\rangle$ and $|f\rangle = |\uparrow\rangle$. The frequency of the incoming light is now chosen such that it drives a non-resonant transition between $|f\rangle$ and $|e\rangle$ with the detuning δ and the coupling constant g . The transition is blind for $|g\rangle$. The light-spin interaction is then described by the effective interaction Hamiltonian:

$$\hat{H}_{eff} = \sum_k g_k |e\rangle \langle f|_k \hat{c} + g_k^* \hat{c}^\dagger |f\rangle \langle e| + \delta |e\rangle \langle e|_k \quad (7.1)$$

With g_k the coupling constant for the k th atom and \hat{c} the annihilation operator for the single field mode light beam. As Andres Sørensen and Klaus Mølmer showed, if we now choose the light resonant with the cavity but far detuned from the atomic transition, the light beam will undergo a phase shift with an angle proportional to the number of atoms in the state $|f\rangle$. By changing the separation of the states and the detuning of the incoming light, the resulting phase shift can be modified.

By choosing the phase shift to be π per atom in the state $|\uparrow\rangle$, we can only distinguish neighboring states, all next-but-one states will be indistinguishable from each other. This leads directly to the situation we discussed for the parity measurement.

This is just one example for an experimental implementation of coarse grained measurements. There are many other effects that could be used for this purpose, e.g. spin-polarization coupling and spin-phonon coupling. All these techniques are already used in experiments or very close to an experimental realization and could be used in the near future to validate the effects of coarse grained measurements.

8 Conclusion

I was able to show, using simulations, that Projective Slot Measurement (PSM) lead to weaker violations of the inequality the larger the slot is (chapter 5). The classical limit could not be reached for the semiclassical measurement: the resulting violation was weak but still present. For higher N and by using coarse-grained POVM it is expected that this violation will vanish. This should be tested in future theses. What my results suggests is that the transition from quantum mechanical to classical description is a continuous one. The exact model for this transition is still not known, but the present data may help finding such a model.

In chapter 6, I could show qualitatively, by using a technique found by Peres, that the longer the slots, the lower the state disturbance. This is another indicator that the slot size for PSM has a big influence on the state that is measured.

Furthermore, I showed by using Random Projection Measurement (RPM), that there are projectors for which the violation of the Leggett-Garg inequality can be higher than in the case of parity measurement and lower than in the semiclassical case. This result was surprising because one could expect that the parity measurement, which separates neighboring states from each other, would be the measurement that displays the quantum character of the system the best. Also one could expect that the semiclassical measurement, which is the closest to a classical measurement would give the lowest possible violation. These effects should be investigated more in future.

Using the state disturbance measurement of Peres I found out that the projectors which lead to a stronger or weaker violation do not lead necessarily to a stronger or weaker state disturbance, respectively. This result might be an indicator that the violation of the Leggett-Garg inequality and the state disturbance, measured with the scheme of Peres, are not equivalent in some cases.

9 Outlook

Coarse grained measurements and their influence on the state during the measurement are a very interesting field of scientific investigation and can lead, for example, to applications in state tomography, where they can help to maximize the ratio of knowledge of a state to the disturbance of the state. But it will be necessary to understand the effects of these measurements more in detail in order to find the right coarse graining for an application. One big step towards this understanding would be the analytical formulation of general coarse grained measurements and their influence on an initial state.

One of the interesting questions to address would be to find out if the states that lead to a higher violation than the parity measurement and a lower violation than the semiclassical measurement can be explained analytically or if they are an artifact of the simulation.

Another interesting task would be to use POVM instead of projective measurements, to see if the violation of the semiclassical case drops to zero and if POVM predicts different effects on the initial state for other slot lengths. A very important and interesting step will be the realization of coarse grained measurements in experiments.

Bibliography

- [1] Johannes Kofler and Časlav Brukner. Classical world arising out of quantum physics under the restriction of coarse-grained measurements. *Phys. Rev. Lett.*, 99:180403, Nov 2007.
- [2] M.A. Nielsen and I.L. Chuang. *Quantum Computation and Quantum Information*. 10th Anniversary Edition. Cambridge University Press, 2011.
- [3] Smite-Meister. Bloch_sphere.svg - wikipedia, the free encyclopedia. http://upload.wikimedia.org/wikipedia/commons/6/6b/Bloch_sphere.svg, 2012. [Online accessed: 11-February-2012].
- [4] A. Einstein, B. Podolsky, and N. Rosen. Can quantum-mechanical description of physical reality be considered complete? *Phys. Rev.*, 47:777–780, May 1935.
- [5] John S. Bell. On the problem of hidden variables in quantum mechanics. *Rev. Mod. Phys.*, 38:447–452, Jul 1966.
- [6] John F. Clauser, Michael A. Horne, Abner Shimony, and Richard A. Holt. Proposed experiment to test local hidden-variable theories. *Phys. Rev. Lett.*, 23:880–884, Oct 1969.
- [7] Bell, J. S. Bertlmann’s socks and the nature of reality. *J. Phys. Colloques*, 42(C2):”C2–41–C2–62”, 1981.
- [8] A. J. Leggett and Anupam Garg. Quantum mechanics versus macroscopic realism: Is the flux there when nobody looks? *Phys. Rev. Lett.*, 54:857–860, Mar 1985.
- [9] A J Leggett. Testing the limits of quantum mechanics: motivation, state of play, prospects. *Journal of Physics: Condensed Matter*, 14(15):R415, 2002.
- [10] Carl A. Kocher and Eugene D. Commins. Polarization correlation of photons emitted in an atomic cascade. *Phys. Rev. Lett.*, 18:575–577, Apr 1967.
- [11] Stuart J. Freedman and John F. Clauser. Experimental test of local hidden-variable theories. *Phys. Rev. Lett.*, 28:938–941, Apr 1972.
- [12] Johannes Kofler and Časlav Brukner. Conditions for quantum violation of macroscopic realism. *Phys. Rev. Lett.*, 101:090403, Aug 2008.
- [13] A. Peres. *Quantum theory: concepts and methods*. Fundamental theories of physics. Kluwer Academic Publishers, 1995.

- [14] A. Kuzmich, N. P. Bigelow, and L. Mandel. Atomic quantum non-demolition measurements and squeezing. *EPL (Europhysics Letters)*, 42(5):481, 1998.
- [15] Anders S. Sorensen and Klaus Molmer. Measurement induced entanglement and quantum computation with atoms in optical cavities, 2003.

List of Figures

2.1	Scheme of the projection.	4
2.2	Illustration of the Bloch sphere.(Illustration taken from [3])	5
3.1	Gedanken experiment with the switches determining experimental setting, detector and source. Alice and Bob each own one experimental setting and one detector.	13
3.2	EPR experiment with photons entangled in polarization. . .	15
3.3	Measurement directions on the bloch sphere.	15
4.1	The macroscopic states with the outcome m in a sharp measurement (black lines) and the measurement precision Δm for (a) a fine grained measurement and (b) a coarse grained measurement.	19
5.1	Measurement under parity coarse graining.	20
5.2	The states are bundled into slots (in this case with length $L=2$) and then projected accordingly onto $P+$ and $P-$	22
5.3	The projection direction for each state is chosen randomly. .	23
5.4	Values of the temporal correlation function depending on the angle of rotation for $N = 11$ and $L = 1$ in blue, $L = 2$ in red, $L = 3$ in green and $L = 6$ in orange.	26
5.5	Values of the violation for the global maximum of the Wigner expression K for different L	27
5.6	The value of K over the rotation angle of the time evolution w for the minimum violation.	29
6.1	Expected probability distribution for a measurement of J_z after a rotation of $\pi/2$ around the x-axis, with $j=32$. (figure taken from [13])	30
6.2	Expected probability distributions for a second measurement of J_z , after one more rotation by $\pi/2$. The results depend on the Δm of the meter which performed the first measurement. From top to bottom,this Δm (shown as a horizontal error bar) is 0, 1, 2, 4, and 8. Different vertical scales are used in the various diagrams, for better visibility. In each diagram, the sum of lengths of the vertical bars is 1, by definition. (figure and caption taken from [13])	31
6.3	Sharp measurement after the first rotation by $\pi/2$. With the total polarized state $ \uparrow\rangle^{\otimes N}$ on the right side of the coordinate system.	32
6.4	Probability distribution of the coarse grain measured state after the second rotation with (a) $L = 1$, (b) $L = 2$, (c) $L = 3$ and (d) $L = 6$. With $N-p+1$ on the x -axis.	33

6.5	Probability distribution of the coarse grain measured state after the second rotation for (a) P_+ given a violation of 0.41922, (b) P_- given a violation of 0.41922, (c) P_+ given a violation of 0.42713, (d) P_- given a violation of 0.42713.	35
6.6	Probability distribution of the coarse grain measured state after the second rotation for (a) P_+ given a violation of 0.00649, (b) P_- given a violation of 0.00649.	35
7.1	(a) Energy levels of atoms with ground state $ f\rangle$ and $ g\rangle$. The cavity couples the state $ f\rangle$ to the excited state $ e\rangle$ with the coupling strength g and detuning δ . $ e\rangle$ decays to $ o\rangle$ with the decay rate γ . (b) Scheme of the experimental realization with two atoms in a cavity. (Figure taken from [15])	36

Zusammenfassung

Während meiner Masterarbeit beschäftigte ich mich mit sogenannten grob gekörnten (coarse grained (CG)) Messungen und deren Wirkung auf quantenmechanische Systeme. CG Messungen können dabei zum Beispiel unscharfe Messungen oder ungewöhnliche Zuordnungen der Zustände zu einem Messergebnis sein, sie sind also so etwas wie die Pixelung der unterscheidbaren Eigenwerte.

Wie Johannes Kofler und Časlav Brukner zeigen konnten [12], können makroskopische Spin Systeme, wie z.B. Elektronenwolken, unter solchen CG Messungen als klassisch betrachtet werden, wenn $\Delta m \gg \sqrt{j}$ gilt, also die Auflösung von unterscheidbaren Eigenwerten Δm schlechter ist als die Quadratwurzel der Länge des Gesamtspins j . Werden solche Systeme allerdings mittels der Paritätsmessung gemessen, eine CG Messung bei der alle Zustände auf zwei Messergebnisse projiziert werden und zwar so, dass immer benachbarte Zustände unterschiedlichen Ergebnissen zugeordnet werden, so sind diese Systeme nur quantenmechanisch erklärbar. Die Unterscheidung zwischen klassischer und quantenmechanischer Erklärung wurde dabei über Einhaltung oder Verletzung der Wigner-Leggett-Garg-Ungleichung getroffen.

Meine Aufgabe bestand nun darin den Zwischenraum zwischen diesen beiden Extremen zu füllen und heraus zu finden wie der Übergang von klassisch interpretierbaren zu nur quantenmechanisch interpretierbaren Systemen abläuft. Dazu erstellte ich ein Mathematica-Programm in dem ich die Resultate der Ungleichung simulierte und verwendete Projective Slot Messungen (PSM), eine projektive Messung bei der zwischen zwei Projektoren unterschieden wird, wobei die Zuordnung der einzelnen Zustände zu den Projektoren durch Slots geschieht. Die einzelnen Slots werden dann den Projektoren zugewiesen, sodass immer benachbarte Slots zu unterschiedlichen Projektoren gehören. Ein Slot kann dabei einen Zustand (Paritätsmessung), zwei, drei, usw., bis zur Hälfte aller Zustände enthalten (semiklassische Messung). Unter Verwendung dieser Projektoren konnte die zeitliche Korrelationsfunktion und der Wert des Wigner-Leggett-Garg Ausdrucks berechnet werden und die Werte verglichen werden. Aus meinen Simulationen lässt sich ganz klar ein Abfall der Höhe der Verletzung der Ungleichung mit der Länge der Slots feststellen. Für die semiklassische Messung konnte allerdings nicht, wie analytisch vorausgesagt, ein Abfall des Wigner-Leggett-Garg Wertes K unter die klassische Grenze gemessen werden. Dies kann an der Tatsache liegen, dass für die vorliegenden Berechnungen projektive Messungen verwendet wurden, im analytisch bewiesenen Fall aber POVM benutzt wurden und dass hier eine relativ kleinen Anzahl an Systemen betrachtet wurde.

Im weiteren überprüfte ich mittels einer zufälligen Zustandszuordnung zu den Projektionsrichtungen (RPM) ob es Projektoren gibt die eine höhere oder niedrigere Verletzung der Ungleichung zur Folge haben. Wie sich zeigte

gibt es eine hohe Anzahl an Projektoren, die die Ungleichung höher verletzen als die Paritätsmessung. Projektoren die eine geringere Verletzung als die semiklassische Messung zur Folge haben sind hingegen weitaus seltener. Im nächsten Schritt wollte ich mir nun die durch die Messung hervorgerufene Störung des Ausgangszustandes genauer ansehen. Dazu benutzte ich ein Verfahren, das Asher Peres [13] erstmals benutzte um zu zeigen wie unscharfe Messungen zu einer geringeren Störung der Ausgangszustände führen können. Dabei wird zunächst eine Zeitevolution des voll polarisierten Ausgangszustandes durchgeführt, anschließend die störende Messung und zum Schluss erneut eine Zeitevolution. Dabei sollte der Zustand ohne die störende Messung durch die beiden Zeitevolutionen in den anderen voll polarisierten Zustand überführt werden, also z.B. von alle Spins nach oben zu alle Spins nach unten.

In meiner Simulation ergab sich nun, dass verglichen mit dem zu erwartenden Ergebnis ohne Zwischenmessung, die Paritätsmessung den Ausgangszustand in eine Superposition aus den voll polarisierten Zuständen überführt, was ich auch analytisch zeigen konnte. Die semiklassische Messung hingegen führt zu einer Anordnung der Wahrscheinlichkeitsverteilung um den ohne Störung zu erwartenden Zustand herum. Dies zeigt, dass je kleiner der Slot, desto größer wird die Störung des Ausgangszustands. Dies stimmt mit den Ergebnissen der Verletzung der Leggett-Gargé-Ungleichung überein.

Eine Überprüfung der Ergebnisse der RPM zeigte allerdings, dass für bestimmte Projektoren eine höhere bzw. niedrigere Verletzung der Ungleichung nicht zu einer höheren bzw. niedrigeren Störung des Systems führen kann. Dies ist als Anzeichen dafür zu werten, dass die Verletzung der Ungleichung und die Störungsmessung nach Asher Peres in bestimmten Fällen nicht äquivalent sind.

Lebenslauf

Persönliche Daten

Name: Matthias Kaiser
Geburtsdatum und -ort: 17.06.1984 in Frankfurt/Main (Deutschland)
Nationalität: deutsch

Schulische Ausbildung

bis 2004 Max-Beckmann-Schule in Frankfurt/Main
Abschluss: Abitur (2,3)

Grundwehrdienst/Zivildienst

2004-05 Zivildienst, Röntgenabteilung der orthopädischen Klinik
Friedrichsheim in Frankfurt/Main

Studium

WS 2005 – SS 2009 Physikstudium an der Goethe Universität Frankfurt/Main
Abschluss: Bachelor of Science (2,3)
WS 2009 – SS 2012 Masterstudium der Physik an der Universität Wien

Praktika

Mehrmalig schulische Praktika im Institut für Kernphysik Frankfurt/Main
September-Oktober 2008 6-wöchiges Praktikum im Institut für Quantenoptik und
Quanteninformation (IQOQI) Wien

Auslandsaufenthalte

Schüleraustausch nach Guangzhou/Guangdong/China
WS 2010 ERASMUS-Aufenthalt in Riga/Lettland